Michalowski, R. L. & Drescher, A. (2009). *Géotechnique* **59**, No. 10, 839–850 [**doi:** 10.1680/geot.8.P.136]

Three-dimensional stability of slopes and excavations

R. L. MICHALOWSKI* and A. DRESCHER†

Three-dimensional (3D) limit analysis of stability of slopes is presented. Such analyses are not common, because of the difficulties in constructing three-dimensional mechanisms of failure in frictional soils. A class of admissible rotational mechanisms is considered in this paper. The failure surface has the shape of a curvilinear cone ('horn'), with upper and lower contours defined by log-spirals; all radial cross-sections of the surface are circular. In the special case of cohesive soils (undrained behaviour), the shape of the failure surface reduces to a torus. An alternative failure surface is generated when the axis of rotation intersects the circle that generates the surface. The 3D mechanism is further modified with a plane-strain central insert to ensure the transition to a plane-strain mechanism if no restraint is placed on the slope width. Also, the spherical failure surface considered in the literature is re-examined. The critical height of slopes with finite width is determined, and the results are presented in the form of graphs and tables for a practical range of parameters. A separate set of results is given for the critical depth of excavations, where the extent of the failure mechanism is defined by the geometry of the earthworks. An example illustrates the practical use of the results.

KEYWORDS: excavations; failure; landslides; limit state design/analysis; plasticity; slopes

Cette communication présente l'analyse limite tridimensionnelle de la stabilité des pentes. Ces analyses ne sont pas fréquentes, en raison des difficultés que présente la construction de mécanismes tridimensionnels de rupture des sols de frottement. Dans la présente communication, on se penche sur une classe de mécanismes rotatifs admissibles. La surface de rupture a la forme d'un cône curviligne (« corne »), dont les contours supérieurs et inférieurs sont définis par des spirales logarithmiques. Toutes les coupes radiales de la surface sont circulaires. Dans le cas particulier de sols cohésifs (comportement non drainé), la forme de la surface de rupture se réduit à un tore. Une surface de rupture alternative est produite lors de l'intersection de l'axe de rotation avec le cercle produisant la surface. Le mécanisme tridimensionnel est également modifié avec un insert central à déformation plane, afin d'assurer la transition à un mécanisme de déformation plane si aucune restriction n'est imposée sur la largeur de la pente. En outre, on procède également à un nouvel examen de la surface de rupture sphérique décrite dans les différents ouvrages. On détermine la hauteur critique des pentes à largeur finie, en présentant les résultats sous forme de graphes et de tableaux pour une gamme pratique de paramètres. Un ensemble distinct de résultats est fourni pour la profondeur critique des excavations, lorsque l'étendue du mécanisme de rupture est définie par la géométrie des travaux de terrassement. Un exemple illustre l'application pratique des résultats.

INTRODUCTION

Analyses of slope stability typically involve plane-strain failure mechanisms for reasons of simplicity, and because such failure modes yield conservative estimates of the slope safety when compared with three-dimensional failure patterns. Such analyses are justified, particularly when the hydraulic conditions and the soil stratigraphy affecting failure are not well defined. However, when the dimensions of a soil slope are clearly limited by neighbouring rock formations or existing structures, a three-dimensional analysis of safety may be more appropriate. This is particularly true in the case of earth works, where the geometry of excavations is well defined, and so are the limits on possible failure mechanisms. Seeking a more accurate prediction of safety in three-dimensional cases could lead to significant savings in the construction of slopes, and to more mechanics-motivated slope design. Also, two-dimensional forensic analyses ('back-calculations') of three-dimensional failures lead to erroneous estimates of the actual soil strength parameters, and the development of a realistic three-dimensional analysis would help to remedy this inaccuracy.

Manuscript received 18 November 2008; revised manuscript accepted 26 March 2009.
Discussion on this paper closes on 1 May 2010, for further details see p. ii.
* Department of Civil and Environmental Engineering, University of Michigan, Ann Arbor, USA.
† Department of Civil Engineering, University of Minnesota, Minneapolis, USA.

The stability of slopes has been addressed by many, and an extensive review of the subject with an emphasis on planar failures can be found in Duncan (1996). Three-dimensional analyses of slopes are less common, and can be grouped into three categories: the extension of traditional slice methods; numerical approaches, such as the finite element method or the discrete element method; and limit analysis (the plasticity approach). The reader will find a review of the first two categories in a recent article by Griffiths & Marquez (2007). The application of limit analysis to earth slopes started with a paper by Drucker & Prager (1952), who applied the kinematic approach of limit analysis to the stability of slopes undergoing plane-strain failure. Both translational and rotational failure mechanisms were considered in that paper. For a frictional/cohesive material, a simple three-dimensional one-block collapse was considered by Drescher (1983), a more complex 3D multi-block mechanism of slope failure induced by a surface load was described by Michalowski (1989), and a rotational mechanism was considered by de Buhan & Garnier (1998). Three-dimensional rotational failure in purely cohesive soils (undrained behaviour) was considered by Baligh & Azzouz (1975), and by Gens *et al.* (1988).

To avoid confusion we define the term *three-dimensional* (3D) as pertaining to failure mechanisms with three-dimensional features, such as spherical or other 'double-curve' surfaces. The term *two-dimensional* (2D) describes analyses with plane-strain deformation and a geometry of the mechanism that does not vary in the direction perpendicular to the plane of deformation. The term 'two-dimensional' does not mean the absence of the third physical dimension,

and the kinematic discontinuities are represented by surfaces in both types of analysis (rather than by surfaces and lines).

This paper is focused on the three-dimensional, rotational failure of slopes in frictional/cohesive soils, and the application of the kinematic method of analysis. The approach is analytic, in that the geometry of an admissible mechanism is described analytically, and the most critical mechanism is found from an analytical or numerical optimisation scheme. The consideration of rotational mechanisms is motivated by the finding of Chen (1975), who argued convincingly that a two-dimensional rotational mechanism in slopes is the most critical failure pattern among the two-dimensional mechanisms. However, three-dimensional analyses are significantly more involved than two-dimensional ones, for the class of admissible rotational mechanisms now is much broader, and, at the same time, it is more difficult to construct and analyse the admissible mechanisms, particularly in the presence of soil friction.

The application of the kinematic method of limit analysis to stability of slopes will be discussed first. Next, a three-dimensional rotational mechanism in slopes with frictional/cohesive soils will be discussed, followed by an analysis of 3D slope failures in cohesive soils with incompressible behaviour (undrained conditions). A special case of a three-dimensional rotational mechanism with a spherical cap failure surface will follow. This case has been considered previously (Hungr *et al.*, 1989; Silvestri 2006; Griffiths & Marquez, 2007), and the analysis presented aims at re-examining the findings. Results for slopes with their width restricted by constraints, such as walls of rock formation, will be presented, and the results for excavations will be given in the penultimate section. The charts in the paper may serve as practical tools for slope stability assessment. The paper will be concluded with final remarks.

KINEMATIC METHOD OF LIMIT ANALYSIS IN SLOPE STABILITY

Limit analysis aims at evaluating bounds on the limit load inducing or resisting failure in structures built of perfectly plastic materials. In application to slopes, the limit load can be identified with forces acting on top of the slope, or the weight of the soil. Alternatively, a bound on the geometry of the slope (e.g. height) can be sought if the unit weight of the soil is given. An upper bound on the load or height can be obtained from the kinematic method, the essential element of which is a kinematically admissible velocity field defining the possible mechanism of failure. The term *admissible* implies that the strain rates resulting from the velocity field must satisfy the flow rule that is associated with the yield condition (strength criterion) of the material, and the velocities satisfy the boundary conditions.

The most common yield condition used for soils is the Mohr–Coulomb function, which contains two material constants: the internal friction angle ϕ and the cohesion intercept c. For purely frictional material $c = 0$, and for purely cohesive soil $\phi = 0$, with the cohesion identified with undrained strength ($c = c_u$). This yield condition is used here to describe the strength of overconsolidated soils. Reduced tensile strength can be accounted for by postulating a tension cut-off. Incorporating this modification, however, increases the complexity of admissible kinematic fields, and is not considered in this paper. Because the flow rule associated with the Mohr–Coulomb yield condition (for soils with $\phi > 0$) predicts larger dilation than that measured in experiments, the non-associated flow rule is often postulated. Although no rigorous bounds on limit loads can be found for non-associated materials, an upper bound for an associated material is also an upper bound for a non-associated one with the same yield condition (Radenkovic, 1962), and this warrants the construction of admissible kinematic solutions satisfying the normality flow rule.

In the case of a three-dimensional and continuous deformation field, the flow rule requires the following relationship among the principal strain rates

$$\dot{\varepsilon}_1 + \dot{\varepsilon}_2 + \dot{\varepsilon}_3 + (\dot{\varepsilon}_1 - \dot{\varepsilon}_2 - \dot{\varepsilon}_3)\sin\phi = 0 \tag{1}$$

The construction of velocity fields satisfying equation (1) is a difficult task, and no solutions other than axisymmetric have been reported in the literature (Drescher, 1986). The task simplifies greatly if the material is purely cohesive ($\phi = 0$), the problem is of the plane strain-type ($\dot{\varepsilon}_2 = 0$), or the failure mechanism is of the rigid-block motion type. In the last case, strain rates are zero within the rigid blocks, and equation (1) is satisfied within blocks identically. The blocks are separated by velocity discontinuity surfaces, which can be interpreted as limits of thin material layers undergoing shear and possibly dilation. When equation (1) is applied to these thin layers, it leads to the condition where the velocity jump vectors must be inclined at angle ϕ to the discontinuities: that is

$$[v_n] = [v_t]\tan\phi \tag{2}$$

where $[v_n]$ and $[v_t]$ are the normal and tangential components of the velocity jump vector $[v_i]$ respectively. This requirement is equally mandatory in two-dimensional and three-dimensional mechanisms. Numerous two-dimensional translational and rotational mechanisms have been considered in the literature for $\phi \geqslant 0$, when the velocity discontinuities are straight lines (planes) or logarithmic spirals (circles for $\phi = 0$). Baligh & Azzouz (1975) and Gens *et al.* (1988) considered three-dimensional rotational mechanisms for purely cohesive soils ($\phi = 0$), for which any surface of revolution is an admissible velocity discontinuity, and the velocity jump vectors are tangential. These surfaces are generated by rotating a straight line or a curve about an axis of rotation parallel to the slope crest: examples are a cylinder, a cone, and a paraboloid. Three-dimensional translational mechanisms with planar surfaces for $\phi > 0$ can be found in Drescher (1983) and Michalowski (1989). Solutions with three-dimensional blocks undergoing rotation for soils with $\phi > 0$ are rare (de Buhan & Garnier, 1998); the discontinuity surfaces in such mechanisms are neither planar nor surfaces of revolution. A class of admissible rotational mechanisms is discussed in this paper.

For a kinematically admissible velocity field an upper bound on the limit load (or on the slope height) is determined by equating the rate of work of external forces W to the rate of work D, dissipated internally in the failure mechanism. This is often referred to as the energy rate balance. With no forces on the slope surface, the rate of external work is provided only by the weight of the soil, and it is calculated as an integral of the dot product of the unit weight vector γ_i and the velocity vector v_i. In rotational mechanisms, the work rate of the weight (W_γ) can be calculated as the dot product of the total weight of a block W_i and the velocity of the block centroid v_i^c

$$W_\gamma = \int_V \gamma_i v_i \mathrm{d}V = W_i v_i^c \tag{3}$$

with V being the volume of the rotating block. In general, the rate of dissipated work D is the sum of dissipation within volume V, D_V, and over the velocity discontinuity surfaces S_t, D_t. In terms of the principal strain rates, the dissipation within the deforming volume can be expressed as

$$D_V = \int_V c\cos\phi(\dot{\varepsilon}_1 - \dot{\varepsilon}_2 - \dot{\varepsilon}_3)\mathrm{d}V \tag{4}$$

whereas for velocity discontinuity surfaces S_t the dissipation rate can be written as

$$\begin{aligned} D_t &= \int_{S_t} c[v_t]\mathrm{d}S_t \\ &= \int_{S_t} c\cos\phi[v]\mathrm{d}S_t \end{aligned} \tag{5}$$

In the case of planar discontinuities (translational mechanisms) it is relatively simple to calculate D_t. It becomes more involved if the boundaries are complex curvilinear surfaces, typical of rotational mechanisms. For materials with $\phi > 0$ an advantageous alternative to the integration given in equations (4) and (5) is use of the methodology suggested by Michalowski (2001). This methodology is based on the observation that, using the divergence theorem, the sum of volumetric strain rates in the failure mechanism can be expressed as

$$\begin{aligned} \int_V (\dot{\varepsilon}_1 + \dot{\varepsilon}_2 + \dot{\varepsilon}_3)\mathrm{d}V &= \int_V \dot{\varepsilon}_{ii}\mathrm{d}V = -\int_V \frac{\partial v_i}{\partial x_i}\mathrm{d}V \\ &= -\int_S v_i n_i \mathrm{d}S \\ &= -\int_{S_t} v_i n_i \mathrm{d}S_t - \int_{S_r} v_i n_i \mathrm{d}S_r \end{aligned} \tag{6}$$

where the surface S bounding the mechanism is divided into kinematic discontinuities S_t and the remaining part S_r; n_i is the outward unit vector normal to surface S, and v_i is the corresponding velocity (the negative sign derives from compressive strain rates taken as positive). Making use of equations (1) and (6), equation (4) can be written as

$$\begin{aligned} D_V &= c\cot\phi \int_S v_i n_i \mathrm{d}S \\ &= c\cot\phi \int_{S_t} v_i n_i \mathrm{d}S_t + c\cot\phi \int_{S_r} v_i n_i \mathrm{d}S_r \end{aligned} \tag{7}$$

At the velocity discontinuity surface S_t bounding the mechanism $v_i = [v_i]$, and the dot product $v_i n_i = -[v_t]\tan\phi$. Thus the first term on the right-hand side in equation (7) is opposite in sign, and equal in magnitude, to the dissipation given in equation (5). This implies that the total dissipation in the mechanism $D = D_V + D_t$ is equal to the second term on the right-hand side in equation (7). In the case of a slope, surface S_r consists of two planar surfaces (part of the top surface of the slope, and the face of the slope). This procedure is equally valid if the mechanism contains kinematic discontinuities within volume V.

Note that equation (7) cannot be used when $\phi = 0$, and the dissipation must be determined from equations (4) and (5), for continuous deformation and for discontinuities respectively.

In evaluating an upper bound to the height H of a slope at failure (*critical height*), it is convenient to introduce a dimensionless group $\gamma H/c$, and seek its minimum as a function of slope geometry and friction angle ϕ. The dimensionless group $\gamma H/c$ is sometimes referred to as the *stability factor*, and it is a reciprocal of the *stability number* $c/\gamma H$, used earlier by Taylor (1937). Alternatively, for a slope of given geometry, it is possible to evaluate the safety factor, defined as

$$F = \frac{c}{c_d} = \frac{\tan\phi}{\tan\phi_d} \tag{8}$$

where c_d and ϕ_d are ('developed') soil strength parameters required for the slope to become unstable. In seeking the factor of safety, the energy balance yields $\gamma H/c_d$ as a function of ϕ_d, and F is determined by using equation (8). Finding F is explicit when $\phi = 0$, and implicit (iterative) otherwise.

THREE-DIMENSIONAL ROTATIONAL FAILURE MECHANISMS IN SLOPES

A class of kinematically admissible three-dimensional rotational mechanisms for slopes is discussed in this section. Both frictional/cohesive and purely cohesive soils are considered.

Frictional/cohesive soil ($\phi > 0$, $c > 0$)

As implied in equations (1) and (2), the plastic yielding of soils with $\phi > 0$ is accompanied by dilation, and this causes difficulties in constructing kinematically admissible fields. More specifically, in a rigid rotation mechanism (no volume changes within the rotating block), equation (2) must be satisfied across the velocity discontinuity surface bounding the rotating volume. Condition (2) means that locally the surface must be tangent to a cone with apex angle 2ϕ and its axis coinciding with the linear velocity v. This condition, however, does not provide a direct indication as to the overall shape of the surface.

Among the various admissible mechanisms a particular class is suggested now in which all radial cross-sections are circular. An example of such a mechanism is illustrated in Fig. 1(a). The linear velocity in the mechanism is a function of radius ρ and angle θ, its direction is perpendicular to radius ρ, and its magnitude is given by

$$v = \omega\rho \tag{9}$$

where ω is the angular velocity about the axis passing through point O. The shape of this mechanism resembles that for continuous and translational velocity fields considered by Michalowski (2001) for evaluating limit load on rectangular footings.

This mechanism has the shape of a curvilinear cone (a 'horn') with apex angle 2ϕ. This surface is smooth (with the exception of the apex), and has one symmetry plane. Only a portion of this surface intersects the slope. The trace of the mechanism (discontinuity surface) on the symmetry plane is described by two log-spirals, AC

$$r = r_0 \mathrm{e}^{(\theta-\theta_0)\tan\phi} \tag{10}$$

and A′C′

$$r' = r'_0 \mathrm{e}^{-(\theta-\theta_0)\tan\phi} \tag{11}$$

with r_0 and θ_0 as shown in Fig. 1(a). With the trace of the surface intersecting the toe point C, angles θ_0 and θ_h, and ratio r'_0/r_0 uniquely determine the location of the 'horn' surface in the space.

The rate of work of the external forces (weight) and the dissipation rate were calculated from equation (3) and the second term of equation (7) respectively. The best (lowest) estimate of ratio $\gamma H/c$ was obtained by varying the ratio r'_0/r_0 and angles θ_0 and θ_h.

The shape of this mechanism can be regarded as being generated by rotating a circle of increasing diameter (shaded area in Fig. 1(a)) about an axis passing through point O outside the circle. If the circle is rotated about an axis

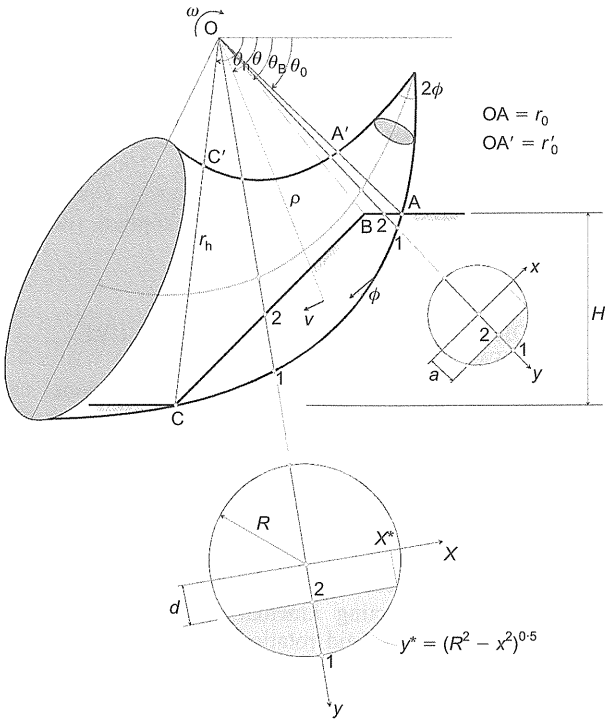

(a)

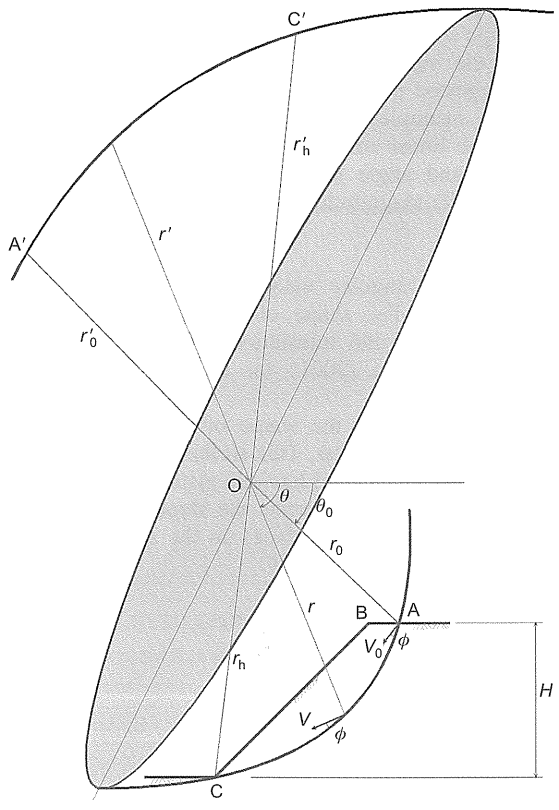

(b)

Fig. 1. Three-dimensional rotational mechanism: (a) a 'horn-shape' surface; (b) alternative mechanism

passing through the circle, a different mechanism is generated (Fig. 1(b)). This time, however, the upper contour A′C′ of the generated block is defined by the log-spiral

$$r' = -r'_0 e^{(\theta-\theta_0)\tan\phi} \tag{12}$$

In the search for the minimum of $\gamma H/c$, the minimisation process for both mechanisms in Fig. 1 can be carried out with the same set of variable parameters: θ_0, θ_h and r'_0/r_0. The ratio r'_0/r_0 assumes positive values for the mechanism in Fig. 1(a), it reaches zero when log-spiral A′C′ reduces to a point at O, and it assumes negative values for the mechanism in Fig. 1(b).

Previous experience (e.g. Duncan, 1996) has shown that plane-strain mechanisms of failure are more critical than three-dimensional ones. Calculations for the mechanisms in Fig. 1 have shown, however, that the minimum ratio $\gamma H/c$ is found at some finite width of the mechanism, even if no constraints are placed on the width of the slope. To allow transition to plane-strain mechanisms, the three-dimensional failure patterns (Fig. 2(a)) were modified with a 'plane insert', by splitting and separating laterally the halves of the 3D surface, as illustrated in Fig. 2(b). This guarantees that in the limit, when the width of the insert $b \to \infty$, the plane mechanism results. This modification introduces one more parameter in the minimisation of $\gamma H/c$, namely the width of the insert, b, with B (Fig. 2(b)) being a given constraint on the width of the mechanism. The plane insert has geometry based on the log-spiral suggested first by Drucker & Prager (1952), and the combined 3D sections and the plane insert form a smooth composite surface. Optimisation of the combined mechanism has shown that an increase in the constraint on the overall width B of the mechanism not only produces a change in the width of the insert, b, but also affects the geometry of the three-dimensional components of the failure surface. Such an insert in three-dimensional failure patterns in frictional soils under footings was considered by Michalowski (2001), to provide a transition from square to strip footings. More details on the equations used in calculations are given in the Appendix.

Cohesive soil (undrained shear strength $c > 0$, $\phi = 0$)

Soils are described as purely cohesive when their shear strength is independent of the level of stress. This is typical

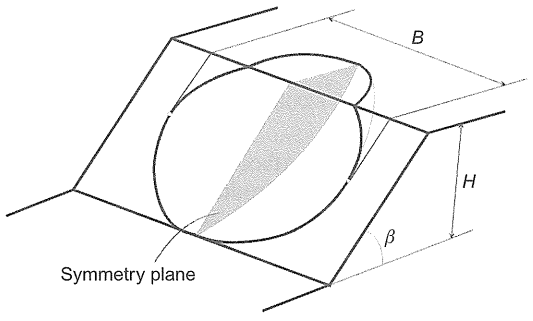

(a)

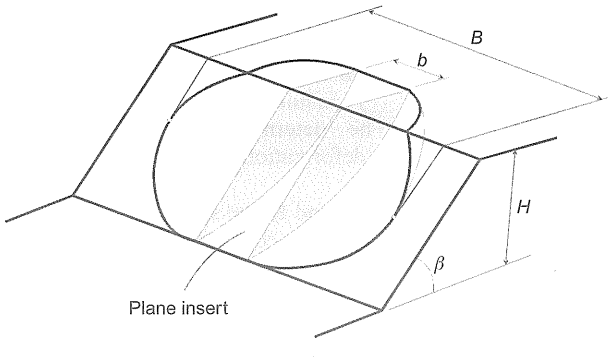

(b)

Fig. 2. (a) Schematic diagram of the 3D mechanism; (b) mechanism with plane insert

of clays subjected to undrained conditions. Constructing rotational mechanisms for such soils is relatively simple, as their deformation occurs without volume change (incompressibility). Consequently, any surface of revolution provides an admissible surface of sliding. An example of such a surface is illustrated in Fig. 3(a). The rotating block has the shape of a portion of a torus, and it is a special case of the first mechanism considered in the previous section. Fig. 3(b) shows the case where the axis of rotation passes through the circle generating the surface. These mechanisms can be modified with cylindrical inserts, to ensure transition to a plane mechanism with an increase in the width of the insert. The mechanisms in Fig. 3 are particular examples of the mechanisms considered earlier by Baligh & Azzouz (1975). Baligh & Azzouz considered a cylindrical mechanism in 'cohesive slopes', with a variety of 'ends' to form an overall three-dimensional mechanism. Similar failure patterns were also considered by Gens *et al.* (1988).

The procedure for computation of the critical ratio $\gamma H/c$ is similar to that for $\phi > 0$, with the exception that the rate of dissipation must now be evaluated from equation (5) rather than equation (7). The details are presented in the Appendix.

Spherical cap failure mechanism

In this section a kinematically admissible rotational mechanism in cohesive soils (undrained behaviour) is considered, with a spherical failure surface confined to the sloping portion of a slope. This is an example that is often considered as a benchmark solution (e.g. Hungr *et al.*, 1989; Silvestri, 2006; Griffiths & Marquez, 2007), and this is a special case of mechanisms considered earlier by Baligh & Azzouz (1975). The problem is sketched in Fig. 4(a), where BAE is the principal cross-section through a spherical cap, and the soil inside the cap rotates about axis z, perpendicular to the plane of Fig. 4(a). The coordinate system used in the calculations is illustrated in Fig. 4(b).

As in equation (3), the work rate W_γ was obtained as the dot product of the soil weight concentrated at its volume centroid G and the velocity vector at G, yielding

$$W_\gamma = \frac{1}{4}\omega\gamma\pi R^4 \cos^4\delta \sin\beta \tag{13}$$

where ω is the rate of rotation about axis z, γ is the unit weight, β is the inclination angle of the slope, and δ is shown in Fig. 4(a). The rate of work dissipation in the mechanism was calculated from equation (5) as an integral of the product of the velocity of points on the cap's surface

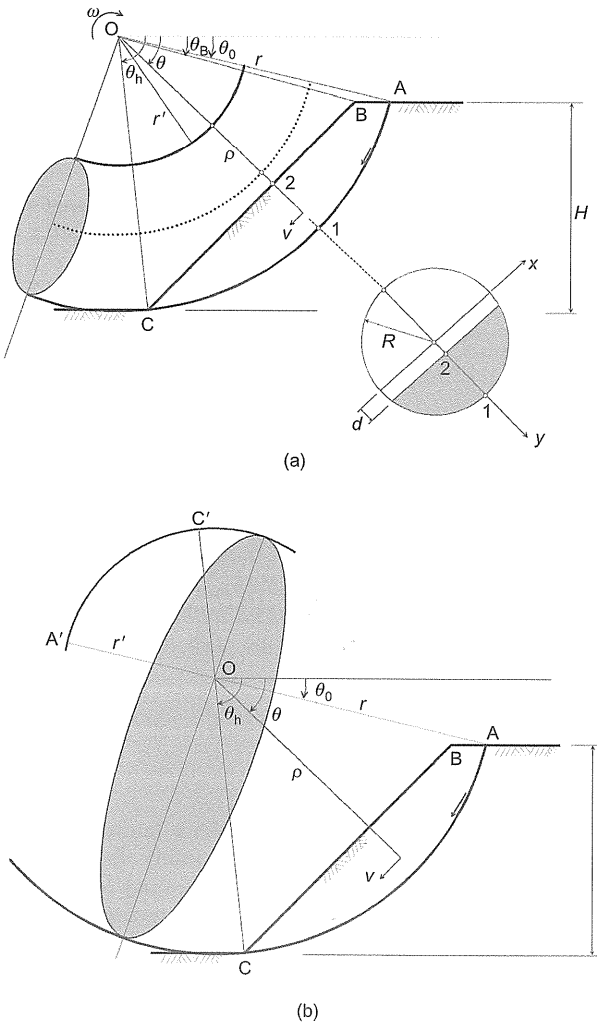

Fig. 3. Rotational failure mechanisms for soil under undrained conditions (incompressible): (a) torus-type failure surface; (b) alternative mechanism

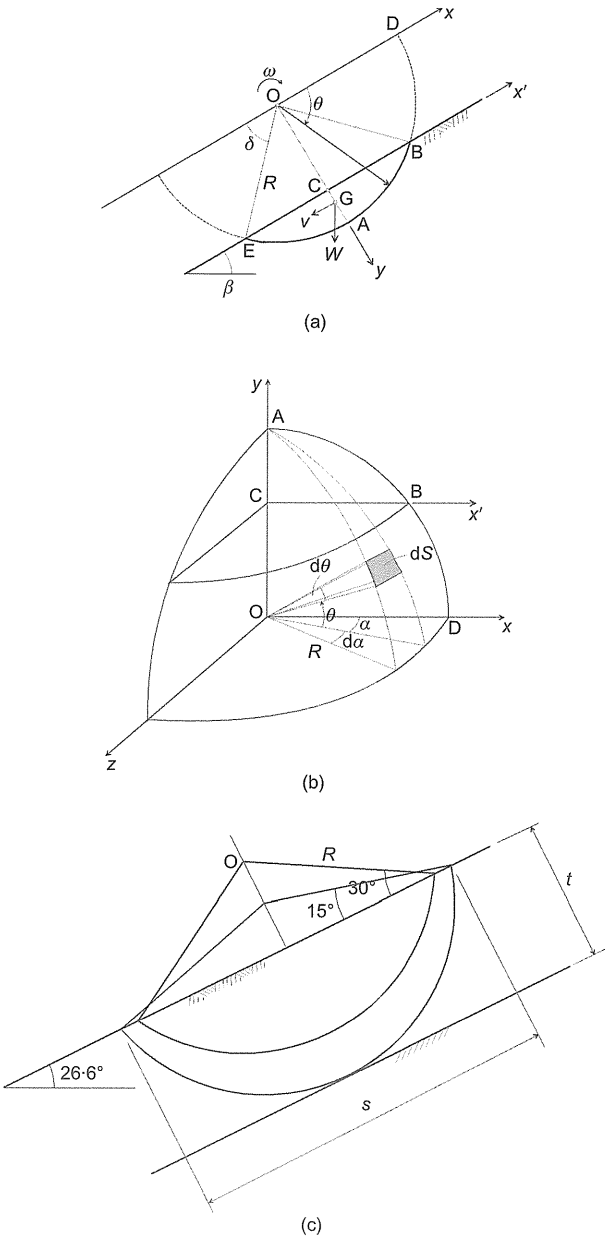

Fig. 4. Spherical cap failure surface: (a) cross-section of mechanism; (b) coordinate system; (c) limit on failure depth

(v) and cohesion (c), taken over the entire cap surface. The velocity v is a function of spherical coordinates θ and α (Fig. 4(b))

$$v = \omega R\sqrt{1 - \sin^2\alpha\cos^2\theta} \tag{14}$$

The infinitesimal area element dS is

$$dS = R^2\cos\theta\, d\alpha\, d\theta \tag{15}$$

and the work dissipation rate becomes

$$D = 4\omega c R^3\int_{\delta}^{\pi/2}\int_{0}^{\pi/2}\cos\theta\sqrt{1 - \sin^2\alpha\cos^2\theta}\, d\alpha\, d\theta \tag{16}$$

Now, comparing equations (13) and (16), an upper-bound estimate of the critical value of $\gamma R/c$ is given by

$$\frac{\gamma R}{c} = \frac{16}{\pi\sin\beta\cos^4\delta}\int_{\delta}^{\pi/2}\int_{0}^{\pi/2}\cos\theta\sqrt{1 - \sin^2\alpha\cos^2\theta}\, d\alpha\, d\theta \tag{17}$$

and the minimum of $\gamma R/c$ is obtained by varying angle δ. For a given γ and c, equation (17) allows determination of the critical value of the radius of the sphere, $R_{cr,}$ for which the slope becomes unstable. Alternatively, a safety factor can be calculated for a slope with given $c/\gamma R$,

$$F = \frac{c}{\gamma R}\frac{16}{\pi\sin\beta\cos^4\delta}\int_{\delta}^{\pi/2}\int_{0}^{\pi/2}\cos\theta\sqrt{1 - \sin^2\alpha\cos^2\theta}\, d\alpha\, d\theta \tag{18}$$

The benchmark solution cited in the literature involves a 1:2 slope ($\beta = 26{\cdot}56°$), $c/\gamma R = 0{\cdot}1$, and one particular angle $\delta = 30°$ (Fig. 4(c)). Many attribute the corresponding solution of $F = 1{\cdot}402$ to Baligh & Azzouz (1975) (e.g. Hungr *et al.*, 1989; Silvestri, 2006; Griffiths & Marquez, 2007), although the specific reference cited does not contain this solution. The limit analysis solution in equation (18), with $c/\gamma R = 0{\cdot}1$ and $\delta = 30°$, confirms the correctness of the referenced safety factor $F = 1{\cdot}402$ for the selected geometric parameters. A value of $F = 1{\cdot}422$ was obtained by Hungr *et al.* (1989) using the limit equilibrium technique, and $F = 1{\cdot}39$ was obtained by Griffiths & Marquez (2007) using a finite element code.

Silvestri (2006) argued that the solution attributed to Baligh & Azzouz (1975) is incorrect, and he presented a different solution ($F = 1{\cdot}377$). However, Silvestri used a rather unusual coordinate system in his integration scheme, and his solution is questionable because of not recognising that the integration limit on θ is a function of ψ in that special coordinate system (specifically, integration in his equation (12) has an incorrect upper limit on θ, and a supposedly typographic error in the exponent of the cosine function).

More generally, equation (18) can be represented in the form

$$F = \frac{c}{\gamma R}\frac{1}{\sin\beta}A_s(\delta)$$

$$A_s(\delta) = \frac{16}{\pi\cos^4\delta}\int_{\delta}^{\pi/2}\int_{0}^{\pi/2}\cos\theta\sqrt{1 - \sin^2\alpha\cos^2\theta}\, d\alpha\, d\theta \tag{19}$$

As angle δ is a free (variable) parameter, the lowest factor of safety F can be found by minimising $A_s(\delta)$. This gives $A_s(\delta)_{min} = 5{\cdot}659$ and the corresponding angle $\delta = 15{\cdot}0°$. On substituting this value, $\beta = 26{\cdot}56°$ and $c/\gamma R = 0{\cdot}1$ in equation (19), $F_{min} = 1{\cdot}265$ is obtained, which is lower than $F = 1{\cdot}402$ for $\delta = 30°$, and the failure mechanism is deeper (Fig. 4(c)). Thus the value listed in the literature is merely a particular value, and not the best upper bound for a given $c/\gamma R$ and slope inclination angle β.

It is further evident from equation (19) that the safety factor for a given slope angle β decreases when the radius R of the spherical cap increases. If the height of the slope is considered infinite, and radius R tends to infinity, the factor of safety tends to zero, $F \to 0$. This is not unexpected as, by definition, an infinite slope can accommodate a failure mechanism of infinite size (radius). Hence considering spherical failure has practical significance only if the extent of the mechanism is restricted to a layer of finite thickness t or distance s (Fig. 4(c)). In the first case the factor of safety can be expressed as

$$F = \frac{c}{\gamma t}\frac{1}{\sin\beta}B_s(\delta)$$

$$B_s(\delta) = \frac{16(1 - \sin\delta)}{\pi\cos^4\delta}\int_{\delta}^{\pi/2}\int_{0}^{\pi/2}\cos\theta\sqrt{1 - \sin^2\alpha\cos^2\theta}\, d\alpha\, d\theta \tag{20}$$

On minimising $B_s(\delta)$, $B_s(\delta)_{min} = 2{\cdot}0$ is obtained and the corresponding angle $\delta = 90°$. In terms of distance s

$$F = \frac{c}{\gamma s}\frac{1}{\sin\beta}C_s(\delta)$$

$$C_s(\delta) = \frac{32}{\pi\cos^3\delta}\int_{\delta}^{\pi/2}\int_{0}^{\pi/2}\cos\theta\sqrt{1 - \sin^2\alpha\cos^2\theta}\, d\alpha\, d\theta \tag{21}$$

and $C_s(\delta)_{min} = 10{\cdot}721$, and $\delta = 23{\cdot}3°$.

If the plane-strain case is considered, and the sphere is replaced by a cylinder, the corresponding expressions for the factor of safety are

$$F = \frac{c}{\gamma R}\frac{1}{\sin\beta}A_c(\delta),\ A_c(\delta) = \frac{3}{2}\frac{\pi - 2\delta}{\cos^3\delta}$$

$$F = \frac{c}{\gamma t}\frac{1}{\sin\beta}B_c(\delta),\ B_c(\delta) = \frac{3}{2}\frac{(1 - \sin\delta)(\pi - 2\delta)}{\cos^3\delta} \tag{22}$$

$$F = \frac{c}{\gamma s}\frac{1}{\sin\beta}C_c(\delta),\ C_c(\delta) = 3\frac{\pi - 2\delta}{\cos^2\delta}$$

and the minimum factors of safety are obtained when $A_c(\delta)_{min} = 4{\cdot}356$ at $\delta = 14{\cdot}1°$, $B_c(\delta)_{min} = 1{\cdot}5$ at $\delta = 90°$, and $C_c(\delta)_{min} = 8{\cdot}280$ at $\delta = 23{\cdot}2°$. Finally, the classical case of a plane-strain infinite slope with a sliding layer of finite thickness t gives

$$F = \frac{c}{\gamma t}\frac{1}{\sin\beta} \tag{23}$$

It was demonstrated that, for slopes with a limited thickness of admissible mechanism, t, the least safety factor is obtained at the limit when $\delta \to 90°$ (i.e. $R \to \infty$) for both the spherical and cylindrical mechanisms. It is noticed, however, that in the limit neither of these rotational mechanisms reduces to the classical plane translational mechanism (equation (23)). When comparing the results above for a given $c/\gamma t$, it is seen that the plane translational mechanism predicts the lowest factor of safety, the rotational cylindrical one predicts a higher value, and the three-dimensional rotational spherical mechanism gives the highest one.

COMPUTATIONAL RESULTS FOR SLOPES

The 3D mechanisms illustrated in Figs 1 and 3 yield the minimum of the critical height $\gamma H/c$ at some finite width of the mechanism in the direction perpendicular to their cross-sections shown. For instance, a slope of 60° in inclination and $\phi = 10°$ reached the minimum of $\gamma H/c$ when the ratio of width B of the mechanism to the slope height was only 1·685. This is not surprising, since the increase of the mechanism width is related to the change in the curvature of the failure surface. To ensure that the mechanism will tend to a plane mechanism when the constraints on its width are not present, a plane section was inserted between two halves of the mechanism, illustrated schematically in Fig. 2(b).

Since the method used in the analysis leads to an upper bound on the critical height $\gamma H/c$, finding the best (least) value of $\gamma H/c$ requires a numerical procedure in which the geometry of the mechanism is varied in the search for the minimum value of $\gamma H/c$. All results presented are based on mechanisms with a plane insert, and the minimum of the dimensionless number $\gamma H/c$ was calculated with independent variable parameters θ_0, θ_h, r_0'/r_0, and the relative width of insert b/H, subject to a limitation imposed on the maximum width of the failure mechanism B/H (Fig. 2).

In the procedure for finding the minimum of objective function $\gamma H/c$, the independent variables were changed sequentially by a small increment in a single computational loop. The loop was then repeated until the minimum was found. Next, the increments applied to the independent variables were reduced, and the process was repeated. The process was stopped when the increments used in optimisation reached 0·01° for θ_0 and θ_h, and 0·001 for r_0'/r_0 and b/H (a typical time to obtain the least upper bound of $\gamma H/c$ for one set of parameters ϕ, β and B/H, was about 10 s using a PC with a 2·83 GHz processor).

The results of optimisation for the undrained analysis (incompressible soil) are presented in Fig. 5(a). The magnitude of critical $\gamma H/c$ has a tendency to increase significantly with the decrease in the width-to-height ratio B/H. For small B/H the mechanisms in Fig. 3 could not be constructed owing to geometrical constraints, and a plane-strain mechanism limited by two vertical planes was used for these cases (Fig. 6(a)). This mechanism is similar to one used by Baligh & Azzouz (1975). Such a mechanism is kinematically admissible for slopes in incompressible soils, and is more critical for a small B/H ratio. For instance, for a vertical slope confined to $B/H = 2·0$, the mechanism in Fig. 3(a) (with the addition of a small insert as in Fig. 2(b)) yields $\gamma H/c = 5·163$, whereas that in Fig. 6(a) gives the value 5·136. For larger B/H the mechanism in Fig. 3(b) (with insert) yields the least upper bound to $\gamma H/c$.

When selecting parameters $r_0'/r_0 = -1·0$, and $\theta_h = \pi - 2\beta - \theta_0$, the mechanism in Fig. 3(b) reduces to a spherical shape as that in Fig. 4(a), leading to a numerical solution identical to that in equation (17).

For dilatant soils (Figs 5(b) and 5(c)) the mechanisms in Fig. 1 (with insert) were used, with the exception of small B/H, where the one-block mechanism (Fig. 6(b)), considered earlier by Drescher (1983), gave better results for vertical slopes. For instance, for a vertical slope, $\phi = 30°$, and $B/H = 0·8$, the mechanism in Fig. 1(a) gave $\gamma H/c = 14·368$, whereas that in Fig. 6(b) yields $\gamma H/c = 12·348$. For $B/H > 1·0$, however, the mechanism in Fig. 1(a) with an insert gave the best estimates of the critical $\gamma H/c$. This mechanism was also the most critical for slopes with inclination less than vertical included in Figs 5(b) and 5(c). Notice that, for very small B/H, admissible mechanisms passing through the toe could not be constructed; one could interpret this result as failure not reaching the toe of the slope (dashed horizontal lines in Figs 5(b) and 5(c)).

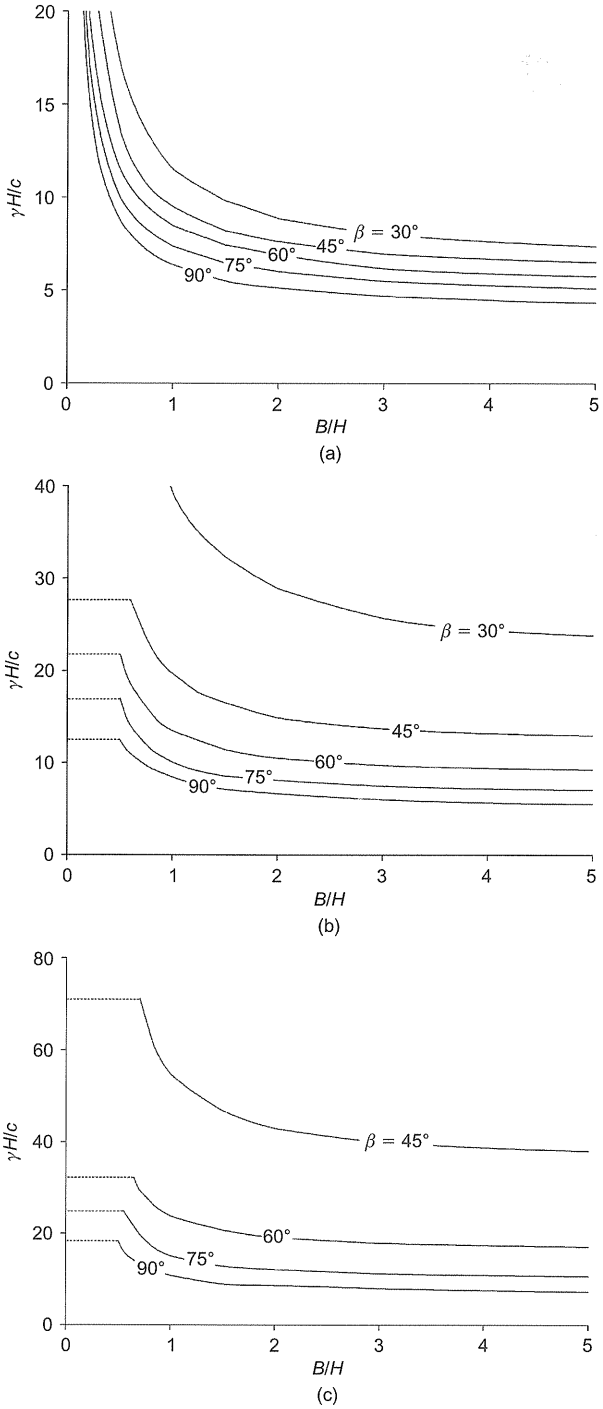

Fig. 5. Critical value of $\gamma H/c$ as function of width of slope: (a) $\phi = 0$; (b) $\phi = 15°$; (c) $\phi = 30°$

The least upper bounds of $\gamma H/c$ calculated for slopes confined to width-to-height ratio B/H are presented in Tables 1 to 3.

STABILITY OF UNSUPPORTED EXCAVATIONS

The extent of slope failure in excavations is constrained by the geometry of the excavation. Excavations of a rectangular plan are considered, with all slopes inclined at one angle β (Fig. 7(a)). The more susceptible to failure is the slope along the larger dimension B^*. B^* is measured at the bottom of the excavation. A trace of the failure mechanism limited by the vertical plane below line CD is illustrated in Fig. 7(b). Examples of critical mechanisms for a $\beta = 45°$ excavation and a vertical cut are illustrated in Figs 7(c) and

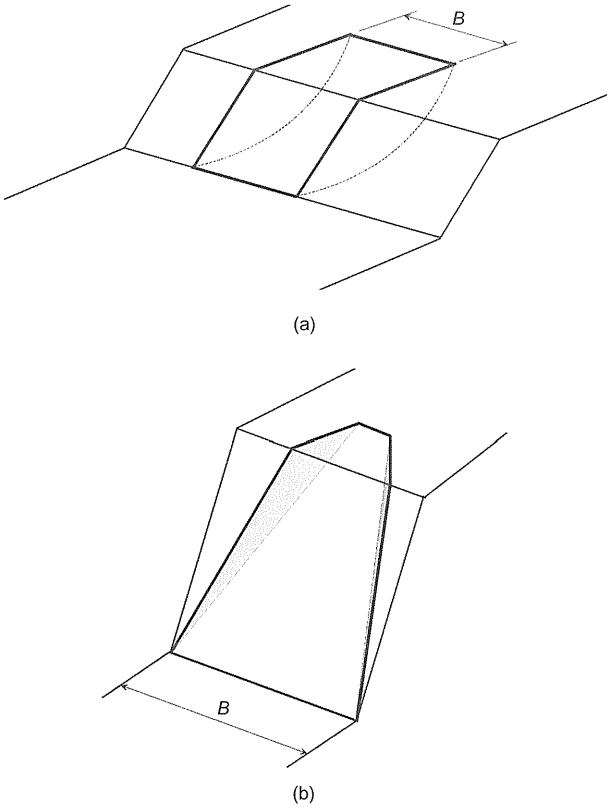

Fig. 6. Simple mechanisms: (a) planar constraints for incompressible soil (Baligh & Azzouz, 1975); (b) one-block mechanism for dilatant soil (Drescher, 1983)

Table 1. Critical values of $\gamma H/c$ for slopes with vertical constraints and incompressible soils ($\phi = 0$)

B/H	β				
	30°	45°	60°	75°	90°
0·5	17·106	13·541	11·484	9·987	8·753
0·6	15·410	12·326	10·493	9·126	7·969
0·8	13·264	10·786	9·241	8·036	6·977
1·0	11·957	9·847	8·478	7·371	6·373
1·5	10·184	8·078	7·441	6·469	5·554
2·0	9·280	7·630	6·897	6·008	5·136
3·0	8·006	6·969	6·163	5·498	4·694
5·0	7·372	6·522	5·758	5·115	4·334
10·0	6·806	6·151	5·473	4·768	4·018

Table 2. Critical values of $\gamma H/c$ for slopes with vertical constraints and $\phi = 15°$

B/H	β				
	30°	45°	60°	75°	90°
0·5	–	–	21·741	16·979	12·428
0·6	–	27·618	18·561	14·048	10·995
0·8	52·325	22·362	15·236	11·372	9·349
1·0	39·136	19·672	13·615	10·071	8·431
1·5	32·347	16·635	11·747	8·564	7·124
2·0	28·911	14·875	10·527	8·167	6·803
3·0	25·693	13·731	9·748	7·502	6·014
5·0	23·843	12·984	9·266	7·077	5·504
10·0	22·691	12·494	8·927	6·809	5·231

Table 3. Critical values of $\gamma H/c$ for slopes with vertical constraints and $\phi = 30°$

B/H	β			
	45°	60°	75°	90°
0·5	–	–	–	18·290
0·6	–	–	23·304	14·960
0·8	63·604	27·664	17·827	12·348
1·0	54·850	23·835	14·701	11·028
1·5	46·845	20·773	12·976	8·935
2·0	42·732	19·103	12·109	8·604
3·0	39·956	17·873	11·184	7·974
5·0	37·994	17·063	10·628	7·266
10·0	36·703	16·527	10·265	6·944

7(d) respectively. The upper portion of the graph represents the trace of failure mechanisms on the horizontal surface of the slope, and the bottom part is the projection of the trace of the failure pattern on the vertical plane. The projection of line CD on that vertical plane is inclined at angle β to the horizontal. Dotted lines separate the plane inserts from the rest of the mechanisms. For vertical slopes the maximum width of the critical mechanism is reached at the crest of the slope, whereas for slopes of smaller inclinations the critical mechanism reaches the limiting plane at some other point, such as point G in Fig. 7(c).

Calculations for all parameters were performed using the mechanisms in Figs 1 and 3, with an insert as indicated in Fig. 7(b). This time, however, the width of the mechanism is restricted by a vertical plane emerging from the excavation corner, with a 45° projection on the horizontal. Independent variables in minimising $\gamma H/c$ were angles θ_0 and θ_h, the ratio r_0'/r_0, and the relative width of the plane insert, b/H. The results are presented now as functions of B^*/H; they are plotted in Fig. 8, and the numerical values are given in Tables 4 to 6.

Application example

To illustrate the practical use of the charts, an example is presented of how to ensure that the required factor of safety for excavation slopes is indeed satisfied. An excavation is planned in soil with parameters $\gamma = 17$ kN/m^3, $\phi = 20°$ and $c = 12$ kN/m^2. The depth of excavation is 5 m, the bottom level of excavation is rectangular, 5×10 m, and all slopes have an inclination of 45° (1:1). The required factor of safety is 1·5.

The charts and tables represent the dimensionless critical height $\gamma H/c$ as a function of the length at the bottom of the excavation to its depth, B^*/H, the inclination angle of excavation slopes β, and the soil internal friction angle ϕ. This function is now written as stability factor $N(\phi_d)$ in terms of the 'developed' strength parameters

$$N(\phi_d) = \frac{\gamma H}{c_d} \tag{24}$$

which allows the safety factor in equation (8) to be expressed as

$$F = \frac{c}{\gamma H} N(\phi_d) \tag{25}$$

The value of $N(\phi_d)$ is interpolated now from Tables 4 and 5, for $B^*/H = 2·0$, $\beta = 45°$, and $\phi_d = \arctan[(\tan\phi)/1·5] = 13·6°$. The value $N = 13·3$ is obtained, and, substituting this value into equation (25), $F = 1·87$ is obtained. Hence the safety factor is not less than 1·5. Finding the exact value of

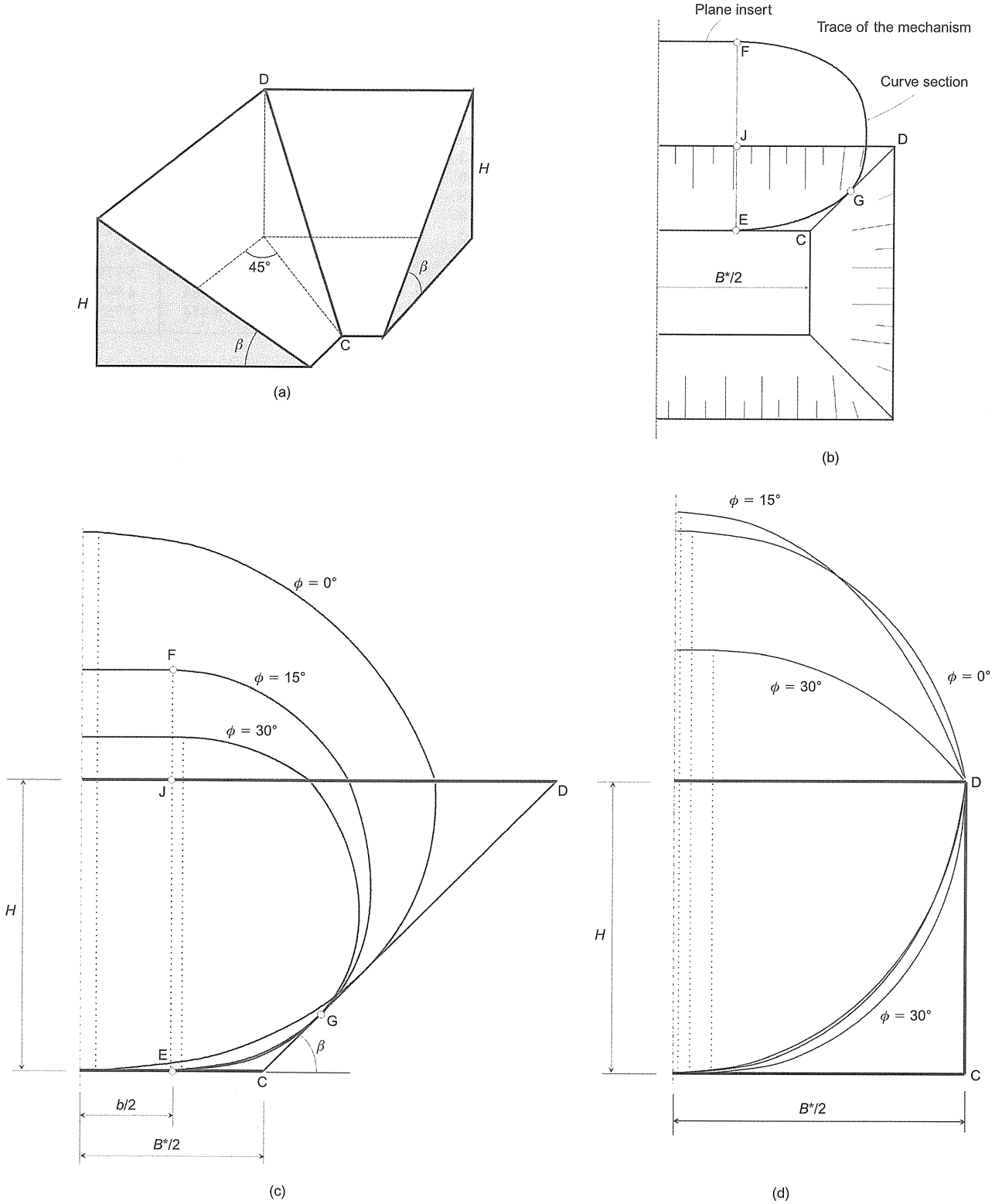

Fig. 7. Excavation: (a) schematic view of excavation corner; (b) plan view; (c) trace of failure mechanism in excavation with slope angles of 45° and $B^*/H = 1{\cdot}25$; (d) mechanism trace for vertical excavation and $B^*/H = 2$

the safety factor, which in this case is in the range 1·5–1·87, requires an iterative procedure. It might be of interest that the critical value of $\gamma H/c$ calculated directly from the computer code for $\phi_d = 13{\cdot}6°$ is $N = 13{\cdot}85$, which confirms acceptable approximation obtained from the linear interpolation.

If the depth of the excavation were to be increased, the ratio B^*/H would decrease, and the factor $N(\phi_d)$ would increase. However, the net contribution of an increase in both $N(\phi_d)$ and H in equation (25) leads to a decrease in the safety factor, as one would expect.

FINAL REMARKS

A three-dimensional rotational mechanism for calculations of stability of slopes in frictional soils was presented. The failure surface is a sector of a curvilinear cone ('horn'), it has a circular radial cross-section, and its lower and upper

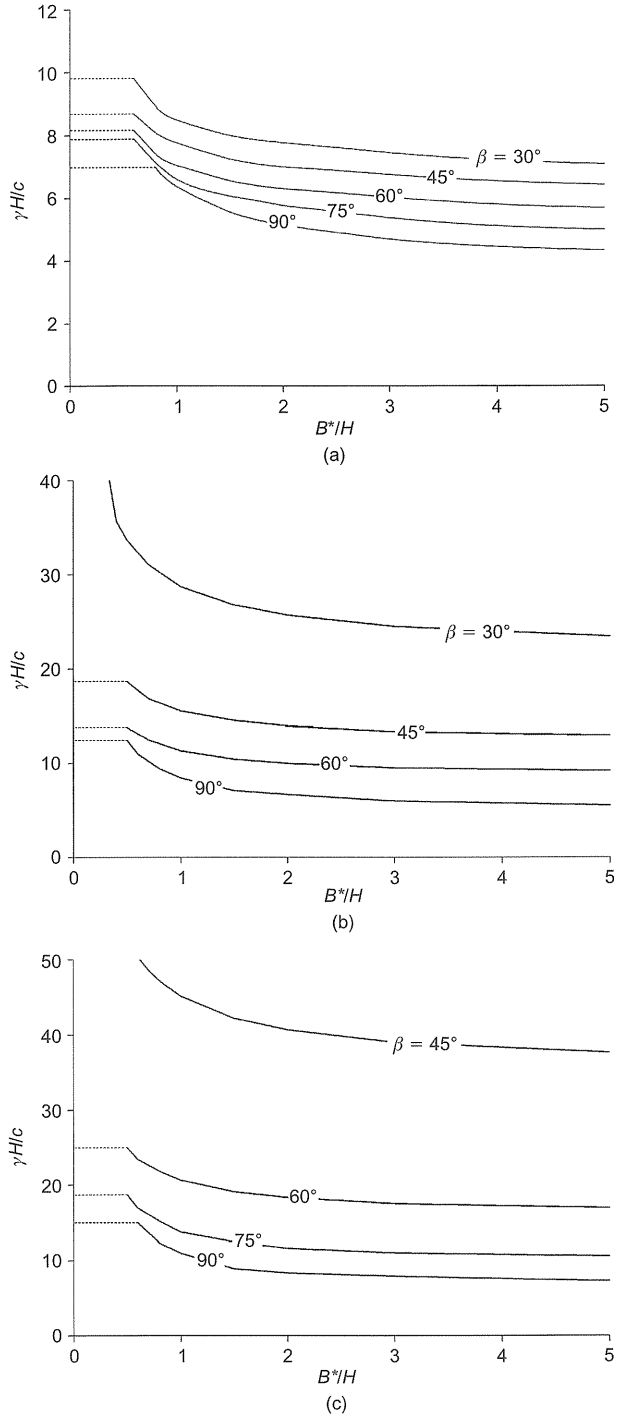

Fig. 8. Critical value of $\gamma H/c$ for unsupported excavations: (a) $\phi = 0$; (b) $\phi = 15°$; (c) $\phi = 30°$

Table 4. Critical values of $\gamma H/c$ for excavations in incompressible soils ($\phi = 0°$)

B^*/H	β				
	30°	45°	60°	75°	90°
0·5	10·359	8·996	8·377	9·987	8·753
0·6	9·801	8·694	8·172	7·887	7·969
0·8	8·936	8·100	7·425	6·993	6·977
1·0	8·652	7·762	7·120	6·564	6·373
1·5	8·067	7·251	6·555	6·074	5·554
2·0	7·764	6·999	6·303	5·761	5·136
3·0	7·456	6·756	6·037	5·379	4·694
5·0	7·093	6·430	5·684	4·997	4·334
10·0	6·754	6·123	5·454	4·755	4·018

Table 5. Critical values of $\gamma H/c$ for excavations in soils with $\phi = 15°$

B^*/H	β				
	30°	45°	60°	75°	90°
0·5	33·687	18·651	13·801	13·254	12·428
0·6	32·454	17·530	13·369	11·724	10·995
0·8	30·109	16·472	12·240	9·770	9·349
1·0	28·708	15·527	11·392	9·293	8·431
1·5	26·786	14·511	10·443	8·600	7·124
2·0	25·697	13·950	9·990	7·850	6·803
3·0	24·496	13·359	9·549	7·371	6·014
5·0	23·449	12·942	9·187	7·039	5·504
10·0	22·596	12·563	8·911	6·813	5·231

Table 6. Critical values of $\gamma H/c$ for excavations in soils with $\phi = 30°$

B^*/H	β			
	45°	60°	75°	90°
0·5	52·945	25·810	18·781	18·290
0·6	50·423	23·413	16·984	14·960
0·8	47·289	21·856	15·225	12·348
1·0	45·193	20·673	13·750	11·028
1·5	42·248	19·093	12·488	8·935
2·0	40·685	18·333	11·636	8·604
3·0	39·050	17·573	11·037	7·974
5·0	37·687	16·963	10·582	7·266
10·0	36·899	16·519	10·255	6·944

contours are defined by log-spirals. The shape of the failure surface is generated by rotating a circle, with increasing radius, about an axis that may or may not intersect the circle. The 'horn' shape is generated when the axis of rotation is not intersecting the circle. The increase in the circle radius is a function of the angle of rotation, and it is adjusted in such a way that the mechanism is admissible for frictional soils.

The mechanism presented is one of a wider class of admissible rotation mechanisms. The cross-section of the mechanism does not necessarily need to be a circle, although the shape of the cross-section (in frictional soils) may not be entirely arbitrary. For instance, a class of polygons with all sides tangent to a circle is another example of an admissible cross-section. In this case, when generating the failure surface, the contour of radial cross-sections preserves its geometrical similarity. Other shapes are also possible, but the cross-section may not conserve its proportions. A general requirement in constructing admissible rotational mechanisms is that, locally, the surface must be tangent to a cone with apex angle 2ϕ and the axis perpendicular to the radial cross-section of the mechanism (i.e. parallel to the linear velocity vector v). For the special case of incompressible soils, $\phi = 0$ (undrained behaviour), any surface of revolution constitutes an admissible discontinuity surface.

The mechanism developed was used to calculate the critical height of slopes. Previous experience indicates that plane-strain failure patterns are more critical than the three-dimensional ones. However, even when the slope width is

not limited, the least upper bound to the critical height determined from mechanisms in Figs 1 and 3 is found for a well-defined width, and the mechanism does not tend to a plane-strain case. For that reason, a plane-strain section was inserted into the mechanism, to ensure transition of the collapse pattern to plane strain, if no bounds are placed on the slope width.

Using the mechanism developed, the critical height ($\gamma H/c$) was calculated for slopes confined to some predetermined width B, for instance due to neighbouring structures. The results are given in this paper for a range of parameters. The width of the failure mechanism is quite naturally a constraint in excavation slopes. A set of results is presented allowing determination of the safety of excavations, given the depth, the inclination of slopes, and the soil properties.

Secondary to the main theme in this paper is a discussion of an existing solution to the safety factor for uniform cohesive slopes with a spherical cap failure surface. This solution is typically given as a function of the radius of the failure surface, because the height of the slope in this problem is not defined (with the exception of the use of FEM). A solution based on kinematic limit analysis is presented. This solution is useful only if the size of the mechanism (spherical cap) is restricted, for instance by limited depth. Without such a constraint the mechanism would increase infinitely, and the factor of safety would tend to zero. Moreover, the spherical cap mechanism is the least critical of the mechanisms considered, and its application might be limited.

ACKNOWLEDGEMENTS

This work was completed when the first author was supported by the Braun/Intertec Visiting Professorship at the University of Minnesota. This support is greatly appreciated. A portion of the material is based upon work sponsored by the National Science Foundation under grant No. CMMI-0724022, and the Army Research Office, grant No. W911NF-08-1-0376.

APPENDIX

With the log-spirals r and r' defining the shape of the 'horn' in Fig. 1(a) given in equations (10) and (11) (or (12)), the centreline of the conical volume $r_m(\theta)$ and the radius of the circular cross-section $R(\theta)$ are found as

$$r_m = \frac{r + r'}{2}$$
$$R = \frac{r - r'}{2} \tag{26}$$

To calculate the work of the soil weight, a local coordinate system x, y was introduced, as shown in Fig. 1(a) (axis x is perpendicular to the plane of the figure). The velocity during rotation about axis O is

$$v = (r_m + y)\omega \tag{27}$$

where ω is the angular velocity, and the infinitesimal volume element is

$$dV = dx\,dy(r_m + y)d\theta \tag{28}$$

The work rate of the soil weight in equation (3) now can be written as

$$W_\gamma = \int_V v_i \gamma_i dV = \gamma \int_V v \cos\theta dV \tag{29}$$

and, more specifically,

$$W_\gamma = 2\omega\gamma \left[\int_{\theta_0}^{\theta_B} \int_0^{x^*} \int_a^{y^*} (r_m + y)^2 \cos\theta \, dy \, dx \, d\theta + \int_{\theta_B}^{\theta_h} \int_0^{x^*} \int_d^{y^*} (r_m + y)^2 \cos\theta \, dy \, dx \, d\theta \right] \tag{30}$$

The two integrals relate to the work rate in the upper portion of the slope, in the range (θ_0, θ_B), and in the remaining part of the slope (θ_B, θ_h). The integration limits along x are $x^* = \sqrt{R^2 - a^2}$ and $x^* = \sqrt{R^2 - d^2}$ in the first and second integral respectively, with R, a and d all being functions of θ (see Fig. 1(a)). Radius R is given in equation (26), and a and d were found from the geometrical relations in Fig. 1(a)

$$a = \frac{\sin(\beta + \theta_h)}{\sin(\beta + \theta)} r_0 e^{(\theta_h - \theta_0)\tan\phi} - r_m$$
$$d = \frac{\sin\theta_0}{\sin\theta} r_0 - r_m \tag{31}$$

The integration limit along y is a function of x, $y^* = \sqrt{R^2 - x^2}$. Angle θ_B was found from trigonometric relations as

$$\theta_B = \arctan \frac{\sin\theta_0}{\cos\theta_0 - A}$$
$$A = \frac{\sin(\theta_h - \theta_0)}{\sin\theta_h} - \frac{e^{(\theta_h - \theta_0)\tan\phi} \sin\theta_h - \sin\theta_0}{\sin\theta_h \sin\beta} \sin(\theta_h + \beta) \tag{32}$$

Before generating the computer program, integration in equation (30) was performed analytically with respect to y and x, and only integration over θ was evaluated using a numerical method.

With the velocity at the boundary points described by ωr (r being the distance from axis O to a point on the boundary), the work dissipation rate given in the second term on the right-hand side in equation (7) can be more specifically written as the sum of the integrals over the surface at the top of the slope (trace AB in Fig. 1(a))

$$\frac{D_{AB}}{c\cot\phi} = -2\omega r_0^2 \sin^2\theta_0 \int_{\theta_0}^{\theta_B} \frac{\cos\theta}{\sin^3\theta} \sqrt{R^2 - a^2} d\theta \tag{33}$$

and the face of the slope (trace BC in Fig. 1(a))

$$\frac{D_{BC}}{c\cot\phi} = -2\omega r_0^2 e^{2(\theta_h - \theta_0)\tan\phi} \sin^2(\theta_h + \beta) \times \int_{\theta_B}^{\theta_h} \frac{\cos(\theta + \beta)}{\sin^3(\theta + \beta)} \sqrt{R^2 - d^2} d\theta \tag{34}$$

The total rate of work dissipation is then $D = D_{AB} + D_{BC}$. Equations (33) and (34) cannot be used for incompressible soils (Fig. 3), and the dissipation for the case $\phi = 0$ was calculated from the following integral over the failure surface

$$D = 2\omega cR \left[\int_{\theta_0}^{\theta_B} \int_a^R (r_m + y)^2 dy\, d\theta + \int_{\theta_B}^{\theta_h} \int_d^R (r_m + y)^2 dy\, d\theta \right] \tag{35}$$

with a and d in equation (31), and θ_B in equation (32). Integration over y was performed analytically, and the integration over variable θ was evaluated numerically. In the special case when $\phi = 0$, both r_m and R in equation (26) are, of course, constant.

The equations presented in this Appendix relate to calculations for the 3D portion of the composite mechanism presented in Fig. 2(b). Including the plane-strain insert requires separate calculations of the work rate of the soil weight in the insert, and the dissipation. These equations are readily available elsewhere (e.g. Chen *et al.*, 1969; Chen, 1975), and are not repeated here. For the plane insert to have a shape consistent with the 3D surfaces, angles θ_0 and θ_h must have identical values in the respective equations for the 3D and the plane insert portions of the failure surface.

REFERENCES

Baligh, M. M. & Azzouz, A. S. (1975). End effects on stability of cohesive slopes. *ASCE J. Geotech. Engng Div.* **101**, No. GT11, 1105–1117.

Chen, W. F. (1975). *Limit analysis and soil plasticity.* Amsterdam: Elsevier.

Chen, W. F., Giger, M. W. & Fang, H. Y. (1969). On the limit analysis of stability of slopes. *Soils Found.* **9**, No. 4, 23–32.

de Buhan, P. & Garnier, D. (1998). Three dimensional bearing capacity analysis of a foundation near a slope. *Soils Found.* **38**, No. 3, 153–163.

Drescher, A. (1983). Limit plasticity approach to piping in bins. *J. Appl. Mech.* **50**, No. 3, 549–553.

Drescher, A. (1986). Kinematics of axisymmetric vertical slopes at collapse. *Int. J. Numer. Anal. Methods Geomech.* **10**, No. 4, 431–441.

Drucker, D. C. & Prager, W. (1952). Soil mechanics and plastic analysis or limit design. *Q. Appl. Math.* **10**, No. 2, 157–165.

Duncan, J. M. (1996). State-of-the-art: limit equilibrium and finite element analysis of slopes. *ASCE J. Geotech. Engng* **122**, No. 7, 577–596.

Gens, A., Hutchinson, J. N. & Cavounidis, S. (1988). Three-dimensional analysis of slides in cohesive soils. *Géotechnique* **38**, No. 1, 1–23.

Griffiths, D. V. & Marquez, R. M. (2007). Three-dimensional slope stability analysis by elasto-plastic finite elements. *Géotechnique* **57**, No. 6, 537–546.

Hungr, O., Salgado, F. M. & Byrne, P. M. (1989). Evaluation of a three-dimensional method of slope stability analysis. *Can. Geotech. J.*, **26**, No. 4, 679–686.

Michalowski, R. L. (1989). Three-dimensional analysis of locally loaded slopes. *Géotechnique* **39**, No. 1, 27–38.

Michalowski, R. L. (2001). Upper-bound load estimates on square and rectangular footings. *Géotechnique* **51**, No. 9, 787–798.

Radenkovic, D. (1962). Théorie des charges limites extension a la mécanique des sols. *Séminaire de Plasticité*, École Polytechnique, 1961, 129–141.

Silvestri, V. (2006). A three-dimensional slope stability problem in clay. *Can. Geotech. J.*, **43**, No. 2, 224–238.

Taylor, D. W. (1937). Stability of earth slopes. *J. Boston Soc. Civ. Engrs*, **24**, No. 3. Reprinted in: *Contributions to Soil Mechanics 1925 to 1940*, pp. 337–386. Boston, MA: Boston Society of Civil Engineers.